Research Journal of Applied Sciences, Engineering and Technology 7(11): 2175-2181, 2014
DOI:10.19026/rjaset.7.513
ISSN: 2040-7459; e-ISSN: 2040-7467

Submitted: October 22, 2012 Accepted: December 20, 2012 Published: March 20, 2014

Research Article

Temperature Field Study on the of Natural Convection and Its Effect on the Critical Speeds in a High Pressure Rotor System

[1]X.Z. Zhu, [1]C.Y. Sun, [2]H.Q. Yuan and [1]Y.D. He
[1]School of Mechanical Engineering, Liaoning Shihua University, Fushun 113001, China
[2]College of Sciences, Northeastern University, Shengyang 110004, China

Abstract: The coupling fluid flow-thermal model of natural convection heat in a High-Pressure Rotor (HPR) of the aero engine was established with Computational Fluid Dynamics (CFD) method. The temperature distributions and flow fields of the HPR with different shutdown time were studied. Then, the temperature distributions of the HPR during the hot start-up with different shutdown time were calculated. Moreover, the effects of hot start-up and shutdown temperature fields on the critical speeds of the HPR were carried out. The results show that the flow rule in the cavity of HPR is different from that in a quadrate cavity and presents diversity and complexity of flow. During 40-90 min of shutdown time, the temperature difference of the HPR is more than 20°C. When the shutdown time reaches to 60 min, the first critical speed of the HPR is decreased by 22.3% from 2256 to 1768 rpm.

Keywords: Aero-engine, CFD, High-Pressure Rotor (HPR), hot startup process, natural convection heat, thermal vibration

INTRODUCTION

Aero-engine rotor system usually works in the conditions of high rotational speeds, non-symmetric and unsteady temperature effect. When the engine is in the cooled state after shutdown, the heat transfer coefficient of natural convection on the upper part of the High Pressure Rotor (HPR) is less than that on the lower part. So the HPR comes into being a strongly non-symmetrical and non-steady temperature field. It results in a larger thermal bending of the HPR. When the aero-engine starts again (hot-start), the HPR forms big vibration amplitudes induced by the non-symmetrical temperature field. In particular, some accidents of the aero-engine often happen because of the big thermal bending during hot startup. For example, the HPR of Olympus 593# aero-engine had a more serious thermal bending at 1.5 h after shutdown. If the aero-engine is forced to hot start up, a serious rubbing fault between the rotor and stator will be formed in the HPR systems (Zhang, 2008). At present, for the aero-engine rotor system, the problem of hot starting up with thermal bending induced by non-symmetrical temperature field has been into "the program of the turbine engine structural integrity" (Zhu *et al*., 2007) and it must be considered in design and test of the aero-engine. To understand thermal vibration response characteristics of the HPR system, we must understand the temperature distributions of the HPR in the condition of natural convection heat transfer. Based on above project background, the natural convective heat transfer inside a certain type of HPR after shutdown is study in this study.

So far, the studies about the natural convection flow and heat transfer focuses on the simply 2D geometric models, such as rectangular enclosures (Girgis, 2000; Sharifa and Liu, 2003; Aounallah *et al*., 2007; Wang *et al*., 2007), vertical plates (Kimura *et al*., 1998; Mendez and Trevino, 2000; Mamun *et al*., 2008, 2009) and the cavities with porous media (Atmane *et al*., 2003; Dong and Li, 2004; Basak *et al*., 2006; Atayılmaz and Teke, 2010; Sankar and Do, 2010). However, these simple models are not fit to study the practical problems, especially for High Pressure Rotor (HPR) of aero-engine. At present, there are not literatures reported the natural convection flow and heat transfer in the real high pressure rotor of aero-engine.

In this study, the CFD model of the HPR is established to study the natural convection flow and heat transfer. The calculated temperature distributions of the HPR at the rotational speed of 1200 rpm are used for the temperature boundary conditions. Based on the Boussinesq hypothesis, the transient velocity and temperature fields in the HPR are firstly studied with different shutdown time under the natural convection. Moreover, the effects of hot start-up and shutdown temperature fields on the critical speeds of the HPR are firstly analyzed. The calculated results provide some theory reference for the thermal deformations and thermal vibration of the HPR.

Corresponding Author: C.Y. Sun, School of Mechanical Engineering, Liaoning Shihua University, Fushun 113001, China, Tel.: +86-413-6865042; Fax: +86-413-6865042

COUPLING FLOW-THERMAL MODEL OF NATURAL CONVECTION

Mathematical model: In this study, the following assumptions are adopted. The incompressible viscous and Newtonian fluid is employed with the Boussinesq hypothesis. The inertia force is neglected because of high viscosity. Based on above assumptions, the basic equations describing the behavior in the Cartesian frame can be written as follows:

The continuity equation can be expressed by:

$$\frac{\partial u}{\partial x}+\frac{\partial v}{\partial y}=0 \tag{1}$$

The momentum equations are defined as:

$$\frac{\partial u}{\partial t}+u\frac{\partial u}{\partial x}+v\frac{\partial v}{\partial y}=-\frac{1}{\rho}\frac{\partial p}{\partial x}+v\left(\frac{\partial^2 u}{\partial x^2}+\frac{\partial^2 u}{\partial y^2}\right) \tag{2}$$

$$\frac{\partial v}{\partial t}+u\frac{\partial v}{\partial x}+v\frac{\partial v}{\partial y}=-\frac{1}{\rho}\frac{\partial p}{\partial y}+v\left(\frac{\partial^2 v}{\partial x^2}+\frac{\partial^2 v}{\partial y^2}\right)+g\beta(T-T_0) \tag{3}$$

The equation of the non-isothermal conservation of energy is given as:

$$\frac{\partial T}{\partial t}+u\frac{\partial T}{\partial x}+v\frac{\partial T}{\partial y}=k\left(\frac{\partial^2 T}{\partial x^2}+\frac{\partial^2 T}{\partial y^2}\right) \tag{4}$$

where,

v and u = The velocities in the x and y directions, respectively
P = The pressure
ρ = The density
g = The gravity
μ = The viscosity
t = The time
T = The temperature
T_0 = The reference temperature
β = The coefficient of thermal expansion

Physical model: Figure 1 shows the 3D geometric model of the HPR. It can be seen that the cavity of the HPR has very complex and symmetry geometric structure, which is completely different from the simple quadrate cavity in natural convection heat transfer. Therefore, we use a two-dimensional and axisymmetric model in Fig. 2 to study the natural convection in the HPR due to its geometrical symmetry.

Figure 3 shows the CFD model of the PHR. The mesh is constructed by using the commercial software, Gambit 3.2. It is noted that the grid should be refined in those regions, such as round solid wall and sudden changed region of flow velocity. The CFD model in Fig. 3 consists of 11,310 cells and 12,442 nodes. The

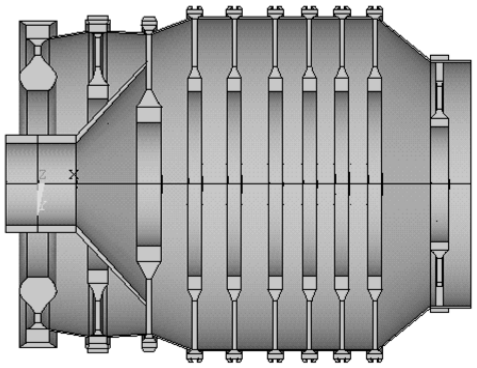

Fig. 1: Three dimensional model of the High Pressure Rotor (HPR)

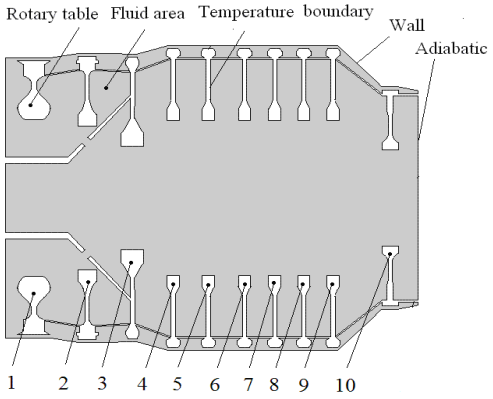

Fig. 2: Geometrical model for nature convection of the HPR 1: Former shaft end; 2: Former inflexion of inclined shaft; 3: Third level disk; 4: Fourth level disk; 5: Fifth level disk; 6: Sixth level disk; 7: Seventh level disk; 8: Eighth level disk; 9: Ninth level disk; 10: Post seal disk

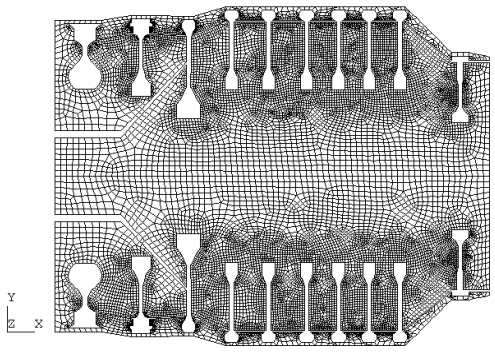

Fig. 3: CFD model of PHR cavity

SIMPLE algorithm is used to solve those equations. The velocity and temperature boundary conditions at top/bottom and left/right sides are given as follows:

Velocities at top/bottom and left/right sides can be described as:

$$v=u=0 \tag{5}$$

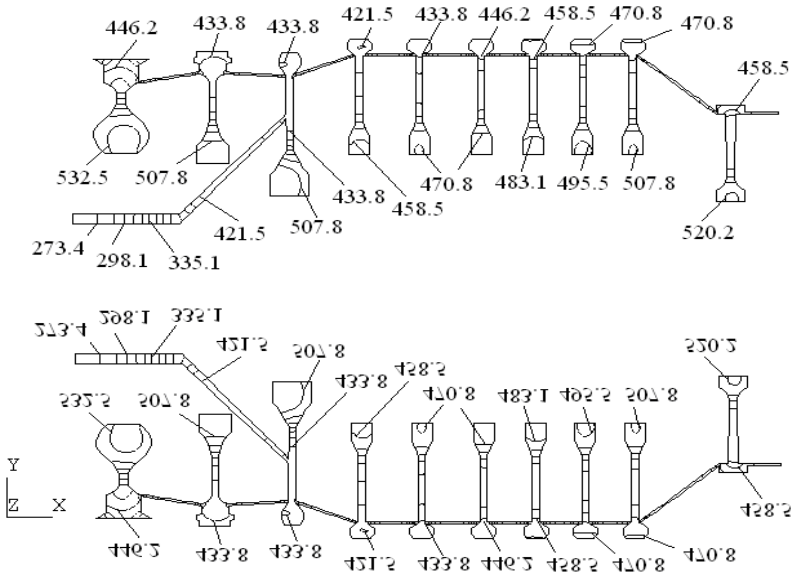

Fig. 4: Boundary condition of initial temperature distributions

Temperature at left/right sides is given as:

$$T = 20°C \quad (6)$$

Temperature at outer surface of top/bottom for the HPR is determined by:

$$T(x, y) = T_f(x, y) \quad (7)$$

where, $T_f(x, y)$ are the calculated temperature values at the rotated speeds of 1200 rpm of the outer surface, as shown in Fig. 4.

RESULTS AND DISCUSSION

Velocity and temperature distributions: Figure 5 presents the velocity distributions in the HPR cavity under the natural convection heat transfer. It can be seen that the calculated velocity distributions of the entire computational domain are very complex because of the complex geometry and temperature boundary conditions. Especially, there are many kinds of vortices between adjacent disks in the cavity. This is mainly because the temperatures in the low-level disks are lower than those in the high-level disks and the temperature difference is the thermal source of air flow in the cavity. In addition, the velocities in upper between adjacent disks of the HPR are more complex than those in lower cavity.

Velocity vectors in the HPR cavity can clearly show the air flow rules of natural convection. Because of the complexities of the geometrical model and big density of grids, it is necessary to be magnified the local regions to better understand the local velocity vectors. The different local regions in the HPR cavity are shown in Fig. 6. And the velocity vector distributions in those regions are shown in Fig. 7.

Figure 7 shows magnified velocity vectors in the different regions from Region A to F for the HPR cavity. As can be seen from Fig. 7a, the flow characteristics in three adjacent upper disks (such as the fifth, sixth and seventh level disks) are similar. They all form vortices in the three upper disks, but the velocities differ slightly. For example, in the high temperature disk cavity, there are three vortices. But there is only one vortex in the adjacent low temperature zone. Figure 7b shows velocity vector distribution in the cavity between first and secondary level disks. When the air flows in the small flow region, most of air flows in the third and fourth level disks and forms the left and right vortices. And there is only a small amount flowing into the small gap of the high pressure rotor. A typical oval eddy between the upper and lower surfaces of the HPR cavity can be observed in Fig. 7c, in which the flow characteristic is similar to the natural convection in a square cavity (Girgis, 2000). In other region such as region D, E and F, the flow characteristics in those regions are similar to above analysis. In short, the HPR has complex geometry and non-linear temperature boundary conditions changed along the axis. This results in the rules of natural convection transfer heat in the HPR are very complex and a lot of vortex are form, which completely different from the simple square cavity in natural convection (Sharifa and Liu, 2003), showing the diversity and complexity of flow vectors.

Figure 8 shows the transient temperature distributions on top of the HPR with different shutdown time. At the beginning of shutdown in Fig. 8a and b, the temperature isolines are high density and temperature values of the HPR are relatively high. Especially, the

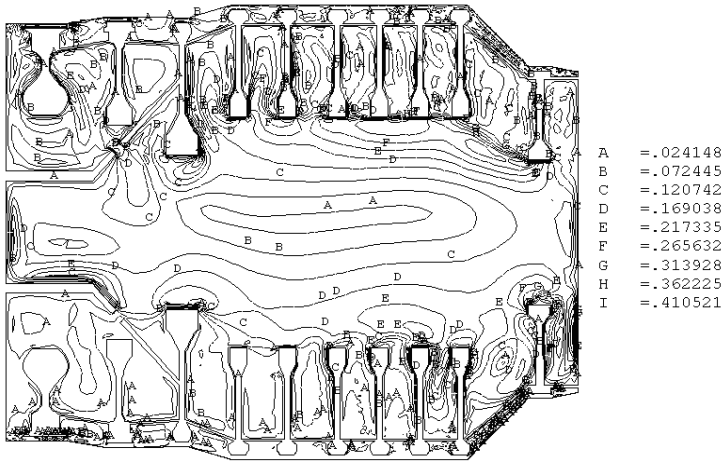

Fig. 5: Velocity distributions in the HPR

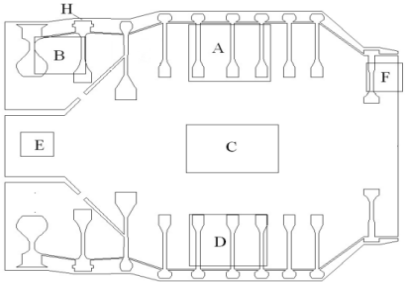

Fig. 6: Positions of different regions in the HPR

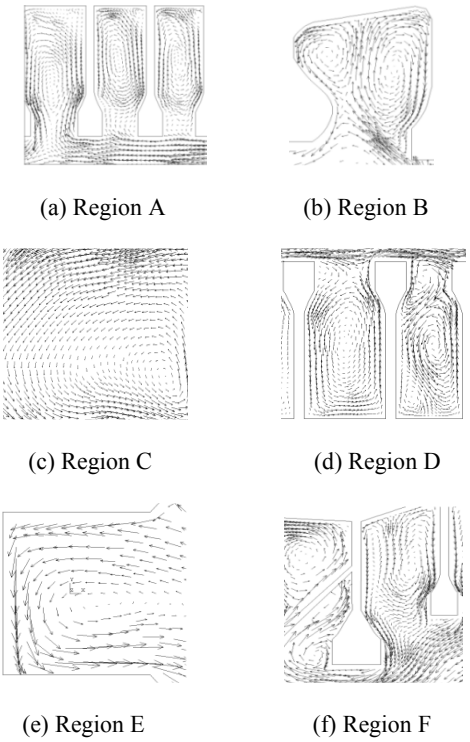

Fig. 7: Velocity distributions of different regions in HPR, (a) region A, (b) region B, (c) region C, (d) region D, (e) region E, (f) region F

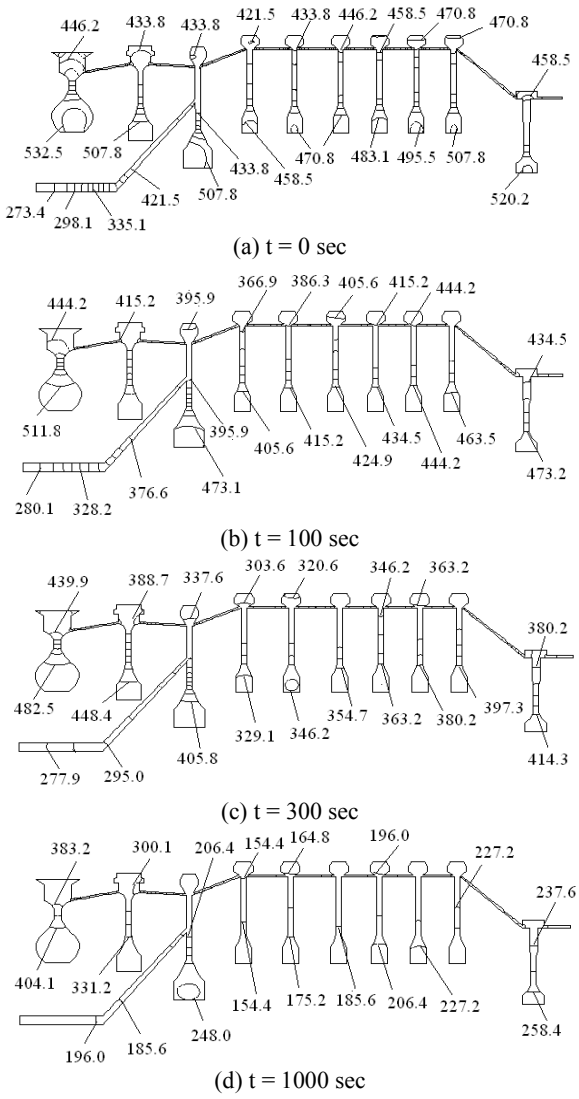

Fig. 8: Transient temperature distributions of HPR with different shutdown time (units: °C), (a) t = 0 sec, (b) t = 100 sec, (c) t = 300 sec, (d) t = 1000 sec

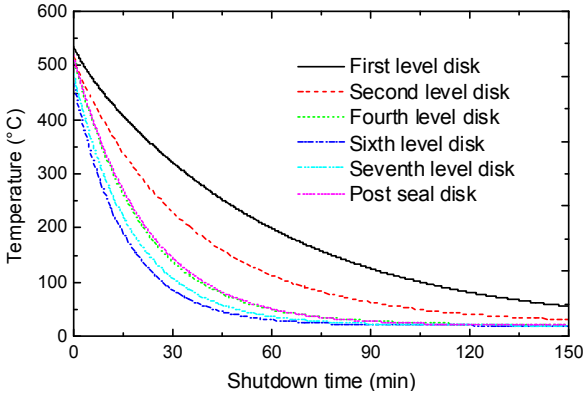

Fig. 9: Temperature curves at different positions with shutdown times

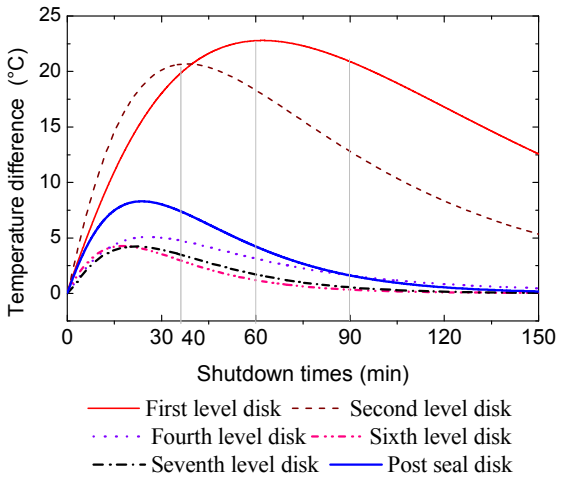

Fig. 10: Difference in temperature curves with different times

third-level and fourth-level disks have large temperature gradient. With increase of shutdown time in Fig. 8c and d, the temperature values and temperature gradients of the HPR gradually decrease. It indicates that the temperature distributions of the HPR are becoming more uniform. By comparison, it is found that the rates of temperature decrease in the third and fourth level disks are relatively small. This is because the velocities and convective heat transfer coefficient in third and fourth level disks are relatively small.

The temperature changes of different positions with different shutdown time are illustrates in Fig. 9. It is observed that the temperatures in all nodes gradually decreased when the shutdown time increases. Meanwhile, the first level disk has the slowest cooling speed and sixth level disk has the fastest cooling speed in all of nodes of the HPR. When the shutdown time goes to 90 min, the cooling speed of each node of the HPR becomes slow. But the first and second level disks still have relative big temperature difference because of the initial high temperatures. At last shutdown time, the temperatures in all nodes of the HPR are equal to the room temperature, which illuminates the heat exchange tends to balance.

Figure 10 depicts the temperature difference between upper and lower surfaces of the HPR with different shutdown time. We can see that the temperatures at top and bottom surfaces of the HPR is not simplified increased with the increase of shutdown time, but show the phenomenon of initial increasing and then decreasing. Meanwhile, the maximum temperature difference between the top and bottom surface is about 23°C at shutdown time of 60 min for the HPR and the minimum temperature difference between the top and bottom surface is about 4.8°C on the sixth level disk at about 15 min. In addition, the temperature difference between the top and bottom surface of the first level disk is relative big and more than 20°C during the shutdown time from 40 to 90 min. It shows a good agreement with the actual measurement values (Zhang, 2008) and verifies the correctness of the simulations in this study. So the HPR come being into relatively strong asymmetric temperature field, which will must change the nonlinear vibration of the HPR system.

Figure 11 shows the temperature curves of different nodes during hot-start process after shutdown time of 300 and 1200 sec. As can be seen from Fig. 10a, when the HPR startups after the shutdown time of 300 sec, the temperature values of the HPR decrease and then gradually increased with the increase of time. The minimal temperature values of different nodes also correspond to the different startup time. Meanwhile, the minimal temperature value of first level disk corresponds to the longest startup time of about 35 sec and that of fifth level disk corresponds to the shortest time of 12 sec. When the shutdown time increases to 1200 sec, as shown in Fig. 11b, the temperature values of the first and second level disks decrease firstly and then gradually increased with the increase of startup time. And other nodes are all increased gradually with the increase of startup time. As the shutdown time increases, the temperature change has tended to balance and the temperature values of all nodes for the HPR equal to room temperature.

Effect of temperature field on critical speeds of the HPR: From above analysis, we have known that the HPR has great temperature changes during the frequent starting and shutdown processes. At the same time, the temperature distributions in each axis section of the HPR are not same each other. Because of the uneven temperature distribution of the HPR, the thermal stresses come into being and lead to some thermal distortion, which results in the change of rigidity matrix and influences the vibration characteristics of the HPR.

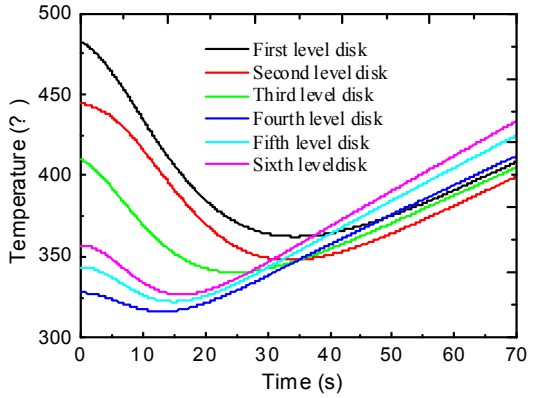

(a) 300 sec

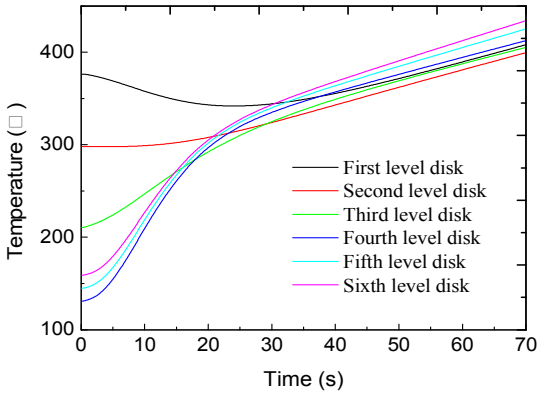

(b) 1200 sec

Fig. 11: Temperature curves of different nodes during hot-start process after different shutdown time, (a) 300 sec, (b) 1200 sec

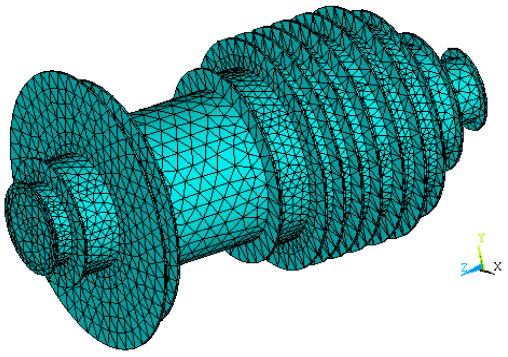

Fig. 12: Three solid dimension finite element mode of HPR

In this section, the effects of nonlinear temperature fields with different shutdown time on the vibration characteristics of the HPR are studied.

According to D'Alembert's principle, the bending vibration equation of rotor system under the action of temperature field can be described as (Zhu *et al*., 2010):

Table 1: Effects of temperature fields with different shutdown time on the critical speeds

Shutdown time (min)	Critical speeds (rpm)				
	1	2	3	4	5
0	2256.5	8189.8	33612.7	50653.9	64025.4
20	1976.5	7499.7	31413.4	48853.2	62639.3
40	1866.6	7256.7	30694.8	48385.1	62278.1
60	1768.3	7010.2	30221.2	47758.0	61740.3

$$[M]\{\ddot{U}\}+[C]\{\dot{U}\}+[K]\{U\}+[K_2]\{U\}=\{P(t)\} \quad (8)$$

where,

$[M]$ = Mass matrix of the rotor system
$[C]$ = Damping matrix including gyroscopic effect
$[K]$ = Stiffness matrix of the rotor system
$[K_2]$ = The stiffness matrix induced by the thermal bending
$\{P(t)\}$ = The thermal stress vector
$\{U\}$, $\{\dot{U}\}$ and $\{\ddot{U}\}$ = The displacement matrix, velocity matrix and acceleration matrix, respectively

Figure 12 shows the three dimensional finite element models of the HPR to calculate the rotor dynamics. The 3D element with 20 nodes is used to mesh the three-dimensional HPR. The FE model of the HPR has 8635 elements and 15874 nodes. In this section, firstly, the steady temperature field of the HPR is calculated based on FEM. Secondly, the thermal stress distributions of the HPR with different shutdown time are studied by using thermal-structure coupled theory. At last, the thermal stress effect reset into the stiffness matrix, the thermal-structure-dynamics coupling equations are employed to study the thermal vibration performance of the HPR.

Table 1 shows the effects of temperature fields with different shutdown time on the critical speeds of the HPR system. During 0~60 min, the critical speeds gradually decrease with the increase of shutdown time due to the increase of temperature difference in the HPR. As the critical speed orders increase, the effects of temperature fields on the critical speeds decrease gradually. When the shutdown time reaches 60 min, the first critical speed decreases by 22.3%.

CONCLUSION

The CFD model of natural convective heat transfer in the HPR is established in the shutdown process. The velocity and temperature field distributions are calculated with different shutdown time. The results show that the HPR has high temperatures at the beginning of shutdown, especially for the third and fourth level disks. With increase of shutdown time, the temperature values in the HPR decrease gradually. When the shutdown time are during 40~90 min, the

temperature difference between the top and bottom surface of the HPR is more than 20°C.

The transient temperature distributions in the HPR are studied during hot starting process after different shutdown time. When the shutdown time is relatively short, temperature values in the HPR initially increase and then decrease. The temperature values of different nodes have different minimal temperature values corresponding to the different shutdown time. Meanwhile, the third-level disk has maximal startup time when its temperature value is lowest, while the eight-level disk has minimal startup time.

The temperature fields with different shutdown time have great effects on the critical speeds of the HPR. During 0~60 min, the critical speeds of the HPR gradually decrease with increase of shutdown time. As the critical speed orders increase from first to fifth order critical speed, the effects of temperature fields on the critical speeds decrease gradually. When the shutdown time reaches 60 min, the first critical speed reduces by 22.3%.

ACKNOWLEDGMENT

The authors gratefully acknowledge that this study was supported by the Science Foundation of Liaoning Educational Committee of China (Project No. L2010247) and Program for Liaoning Excellent Talents in University (No. LJQ2013041). The authors would like to express their appreciation.

REFERENCES

Aounallah, M., Y. Addad, S. Benhamadouche, O. Imine, L. Adjlout *et al*., 2007. Numerical investigation of turbulent natural convection in an inclined square cavity with a hot wavy wall. Int. J. Heat Mass Tran., 50(9-10): 1683-1693.

Atayılmaz, S. and I. Teke, 2010. Experimental and numerical study of the natural convection from a heated horizontal cylinder wrapped with a layer of textile material. Int. Commun. Heat Mass, 37(1): 58-67.

Atmane, M.A., V.S. Chan and D.B. Murray, 2003. Natural convection around a horizontal heated cylinder: The effect of vertical confinement. Int. J. Heat Mass Tran., 46: 3661-3672.

Basak, T., S. Roy, T. Paul and I. Pop, 2006. Natural convection in a square cavity filled with a porous medium: Effects of various thermal boundary conditions. Int. J. Heat Mass Tran., 49(7-8): 1430-1441.

Dong, S.F. and Y.T. Li, 2004. Conjugate of natural convection and conduction in a complicated enclosure. Int. J. Heat Mass Tran., 47(10-11): 2233-2239.

Girgis, I.G., 2000. Numerical and experimental investigations of natural convection in inclined air enclosures. AIAA J., 1: 10-13.

Kimura, S., A. Okajima and T. Kiwata, 1998. Conjugate natural convection from a vertical heated slab. Int. J. Heat Mass Tran., 41(15): 3203-3211.

Mamun, A.A., Z.R. Chowdhury and M.A. Azim, 2008. Conjugate heat transfer for a vertical flat plate with heat generation effect. Nonlinear Anal. Model, 13(2): 213-223.

Mamun, M., S.C. Paul and M.A. Hossain, 2009. Natural convection flow from a horizontal circular cylinder with uniform heat flux in presence of heat generation. Appl. Math. Model., 33(7): 3226-3236.

Mendez, F. and C. Trevino, 2000. The conjugate conduction natural convection heat transfer along a thin vertical plate with non-uniform internal heat generation. Int. J. Heat Mass Tran., 43(12): 2739-2748.

Sankar, M. and Y. Do, 2010. Numerical simulation of free convection heat transfer in a vertical annular cavity with discrete heating. Int. Commun. Heat Mass, 37(6): 600-606.

Sharifa, M.A.R. and W. Liu, 2003. Numerical study of turbulent natural convection in a side-heated square cavityat various angles of inclination. Numer. Heat Tr. A-Appl., 43(7): 693-716.

Wang, G., M. Zeng, Z.P. Huang and Q.W. Wang, 2007. Numerical study of natural convection heat transfer in a porous cavity under time periodic boundary conditions. Chinese J. Comput. Phys., 24(3): 282-286.

Zhang, L., 2008. Analysis of typical aeroengine vibration fault related to thermal bending rotor. J. Vib. Shock, 27(s): 7-9.

Zhu, X.Z., H.Q. Yuan and W. He, 2007. Effect of steady thermal field on critical speeds of a rotor system. J. Vib. Shock, 26(12): 113-116.

Zhu, X.Z., H.Q. Yuan and L. Dong, 2010. Friction thermal effect on rubbing response of a high pressure rotor system. J. Propul. Technol., 37(3): 366-371.